Point-by-point reply from van Ramshorst et al. (2019) to:
Review report: Wind speed measurements using distributed fiber optics: a wind tunnel study

Author of the paper: van Ramshorst et al.
Journal: Atmospheric Measurement Techniques
Manuscript DOI: 10.5194/amt-2019-63

General Comments

The study of van Ramshorst et al. investigated the actively heated fiber-optic (AHFO) technique and estimated its accuracy and precision under controlled airflow conditions by comparing to a three-dimensional ultrasonic anemometer. A valuable error prediction equation for the wind speed measurements at different heating rates was developed, as the heating rate can be a limiting factor for long cables. This equation is also accounting for averaging over space or time which further increases precision. They conclude that AHFO measurements are reliable in outdoor deployments when correcting the measurements for directional sensitivity with an ultrasonic anemometer, choosing the right heating rate and spatial or temporal averaging.
Distributed temperature sensing (DTS) measures temperatures along a fiber-optic cable spatially continuously and can be used in various fields. Especially for atmospheric research this technique offers new insight into the temperature field and thus was implemented in many studies. By using the AHFO technique, wind speed measurements can be added to the system. As the community using the DTS and AHFO technique is growing, the study of van Ramshorst et al. is important for users to be aware of the accuracy, precision and limitation of this technique. Hence, the paper is valuable for our community.

The manuscript improved substantially. It is well organized and leads the reader through the whole manuscript. I still have one major point: The manuscript proposes to develop an error prediction function being valid for any kind of setup. However, the error prediction function is not tested or validated with the existing data set nor is the last point discussed accordingly. I did get a table in the authors' response to compare different approaches of the error prediction function, however, this table is not well explained. Further, no values derived from the prediction function is compared to actually measured quantities neither in the table nor in the manuscript. As the error prediction function is one main goal of the manuscript, either the authors need to explicitly state that the error prediction function needs to be validated in another experiment or another section validating the error prediction function is added to the manuscript. I recommend to accept the submitted manuscript after major revisions. More detailed comments are given below.

Thanks you for the positive feedback, we will give a point-by-point answers to your comments and questions below.

Detailed comments

- p3 l23: Terror: measurement error? how determined?

The measurement error is defined by the machine specifications. We added a line to clarify.

- p3 l27: choose dominant or important or be more specific

We meant dominant, and changed this.

- p8 l18-31: nicely done!

Thanks

- p9 l4: "duplexing" -> duplexed FO core (I would stick with the earlier already mentioned phrase)

We changed this accordingly.

- p9 l6-8: the argumentation to treat the 90° angle different than the others is a bit thin in my eyes: maybe speculate why the 90° angle had lower precision (sharper bending of the FO cable maybe?) and thus justify your decision. Or treat all attack angles the same and shorten all data down. Why should the splice only affect the 90° angle? What if the others were also affected just a bit less?

We clarified possible causes in the manuscript by mentioning the sharper bend and the effect of fixation of the cable. The splice is a different issue and we don't argue that this causes the difference.

- p9 l12-14: "indicating and..." -> "indicating an"; How is the actual spatial resolution defined? Nyquist-frequency?

We use the 10-90% rule to determine the spatial resolution as described in: Tyler, S. W., J. S. Selker, M. B. Hausner, C. E. Hatch, T. Torgersen, C. E. Thodal, and S. G. Schladow (2009), Environmental temperature sensing using Raman spectra DTS fiber-optic methods, Water Resour. Res.,45, W00D23, doi:10.1029/2008WR007052. We clarified this in the paper.

- p9 l14-17: I think mentioning the goal of an error prediction function is more useful than already mentioning the unique constant which is used in the error prediction function later. This will make it easier for the reader to follow your manuscript. Especially the last sentence is confusing to me. Is one constant more representative if I am averaging, but if I am not averaging, it isn't?

We clarified this in the manuscript. We mean that by averaging it becomes more accurate, we changed this accordingly.

- Figure 3, B1, B2: a 1:1-line would be very helpful

We agree and added this to the figures

- Figure B2 and p11 l1-5: It would be easier if B2 has two figures a) 1-s data and b) 30-s data. It is impossible for the reader to combine all four plots in B1 into one plot and compare it to Figure B2.

We agree and created a figure B2 a and b.

- Figure 4: Why is accuracy of 90° & ΔT = 2K getting worse for higher averaging time? I would suspect the opposite as also proposed by the manuscript (p11 l16-17). I would like that this is at least mentioned/discussed.

First of all, we need to clarify that a bias of 0, not necessary means it is perfect. This would assume the energy balance is perfect, however this is not the case as mentioned in the paper. This "error" is most likely different for each angle and heating rate. Secondly all the measurements show the same behavior, they all "drop" for times higher than 1. We see a bigger drop if the ΔT is smaller, which relates to the signal to noise ratio. Finally, the drop for the 90° measurement is bigger because we only have 5 instead of 10 measurements, which doubles the drop in the bias. This shows the precision also has an effect on the bias.

Summarizing:

$$\sigma_a = \frac{(\bar{u}_{DTS}(j) \pm \varepsilon) - \bar{u}_{sonic}(j)}{\bar{u}_{sonic}(j)}$$

With ε being dependent on the precision and error in the energy balance.

- p11 l4: coefficients of determination: I guess that is a linear regression and you show the R-values? What is the derived slope and offset? Please also add this information or at least add the 1:1-lines to the graphs if slope is close to unity anyway.

We plotted the 1:1 line in the figures. Also we clarified the slope and offset in the manuscript and the values are indeed the r^2 (coefficient of determination).

- p11 l16-17: You need to discuss this statement further and use another phrase for "extensive calibration" which is not accurate as different calibration methods can be applied to the FO measurements before even computing wind speeds. I would also argue that maybe the temperature signal needs to be averaged over time before computing the FO wind speed. Would that also increase the accuracy? If not, why? Was this also tested?

We rephrased this sentence into further analysis. Further analysis can be done on improving the energy balance. Considering your second suggestion by averaging over time, this is how we did it.

- p11 l18: I would argue that the dependence between accuracy and averaging time is less pronounced than the one between the precision and averaging time scale, not that the accuracy is constant over time. Besides, it is confusing that σa is given in percent while σp is given in decimal numbers, but percentage values are given in the text. Please make uniform for both parameters.

We changed the sentence into fairly constant. Also we changed all σ's to decimal numbers.

- p11 l20: The last sentence is redundant. Either comment in further detail what Eq. 13 is stating and what dependencies can be determined from Figure 5 or remove the sentence.

We removed this sentence

- p12 l1-3: The meaning of those sentences for the analysis is hard to understand. Further, is j used instead of the measured usonic?

We clarified these sentences by:

For the calculation of the precision u_{DTS}, we considered the natural variability of the wind. We assumed that this natural variability is measured by the sonic and we assume that this per definition is smaller than the variability of the DTS. After applying eq. 13 the variability of the DTS machine u_{DTS} are obtained.

j indicates the wind speed setting, while calculating the actual measured wind speeds are used.

- p12 l6: rephrase: "the precision was averaged over all wind speeds which is justified, because σp is normalized by the mean wind speed, hence any linear dependency should be removed" or similar; "... for all ΔT..." -> "... for each ΔT..."
- p12 l7: "..., with ..." The sentence is redundant to some degree. The colors and symbols are already showing why there are 12 different points for each ntime.

We rephrased these two sentences into:

The precision was averaged over all wind speeds for each ΔT and angle combinations in Figure 5, which is justified because σp is normalized by the mean wind speed, hence any linear dependency should be removed.

- The following is only a suggestion/thought: What about dropping the attack angles for σp? They are not further discussed as you already account for them in the earlier section. So should that maybe not be considered moving on? It is kind of distracting from the main object of different heating rates and averaging time/spatial scales.

We think it is valuable to show the variability between the angles.

- Figure 6a: y-axis label is not representing what is actually plotted: $\sigma_p \frac{\Delta T}{T_{error}}$

We changed this.

- p13 l10-15: If this statement is true, then it needs to be further discussed and why it can be applied to different settings. The statement is also referring to an Equation which is introduced later in the manuscript. So I suggest to insert this paragraph at the corresponding location to Eq. 21 and into Section 3.4, respectively. Also Cint has a wide spread and needs to be further discussed. Again I suggest to insert a plot using the prediction function for σp and the actual derived σp for all averaging scales to show the strength and accuracy of the prediction function.
- Figure 6b: same y-axis problem as Fig. 6a. Further, how can you justify that your proposed constant has a spread from 1.1 to 2.2? This needs to be mentioned and discussed.

We created a new subsection in Section 3.4 showing the validation of our prediction equation. Additionally, we also discuss the sensitivity of the constant C_{int}. The following (subsection) is added to the manuscript:

*"**Verification of the precision prediction section:***

For verification purposes the calculated precision (Eq. 15) is combined with the predicted precision (Eq. 21) in Figure 8. As can be seen in Figure 8 we underestimate the precision of the AHFO system using C_{int}=1.6, meaning that better performance can be expected. This difference can be explained by three causes. First, in Figure 6b it is visible that the 90° data is only averaged over 5 data points instead of 10, resulting in a higher C_{int}. Second, we see the effect of ΔT: how higher the heating the less spread in the precision distribution (Figure 5). Third, we neglect the smaller energy terms in Eq. 19, which leads to an increased σp. To investigate the sensitivity of using a constant C_{int}, the 98% confidence bounds (two times standard deviation) of C_{int} are determined. It is projected (dotted lines) in Figure 8 that the calculated precision is within the 98% confidence interval of the predicted precision. Concluding, with our prediction equation we can predict all our settings within a 98% confidence interval, showing the general applicability."

- p14 l6-7: This is a contradiction as Figure 5 is showing the exact opposite: Higher σp for lower ΔT, lower σp with increasing ntime. σp can be estimated from those variables, but σp is not independent of those.

We understand the confusion; our sentence was wrongly stated. We clarified this in the manuscript by: "... behaves similar for each…." instead of independent.

- Section 3.5: Maybe dew fall on the fiber needs to be considered? Water droplet on the fiber will for sure affect the measurements altering the heat loss of the unheated fiber (assuming the water droplets quickly evaporate from the heated fiber).

We agree and added a part about wet fibers.

- p17 l10: directional sensitivity compensation can only be applied if the angle of attack is known demanding ancillary measurement devices. Please add.

We added this.

Revisiting wind speed measurements using actively heated fiber optics: a wind tunnel study

Justus G.V. van Ramshorst[1,4], Miriam Coenders-Gerrits[1], Bart Schilperoort[1], Bas J.H. van de Wiel[2], Jonathan G. Izett[2], John S. Selker[3], Chad W. Higgins[3], Hubert H.G. Savenije[1], and Nick C. van de Giesen[1]

[1]Delft University of Technology, Water Resources Section, Stevinweg 1, 2628 CN Delft, The Netherlands
[2]Delft University of Technology, Geoscience and Remote Sensing, Stevinweg 1, 2628 CN Delft, The Netherlands
[3]Oregon State University, Biological and Ecological Engineering, 116 Gilmore Hall, Corvallis, Oregon 97331, USA
[4]University of Göttingen, Bioclimatology, Büsgenweg 2, 37077 Göttingen, Germany

Correspondence: Justus van Ramshorst (justus.vanramshorst@uni-goettingen.de)

Abstract. Near-surface wind speed is typically only measured by point observations. The Actively Heated Fiber-Optic (AHFO) technique, however, has the potential to provide high-resolution distributed observations of wind speeds, allowing for better spatial characterization of fine-scale processes. Before AHFO can be widely used, its performance needs to be tested in a range of settings. In this work, experimental results on this novel observational wind-probing technique are presented. We utilized a controlled wind-tunnel setup to assess both the accuracy and the precision of AHFO under a range of operational conditions (wind speed, angles of attack and temperature difference). The technique allows for wind speed characterization with a spatial resolution of 0.3-m on a 1-s time scale. The flow in the wind tunnel was varied in a controlled manner, such that the mean wind, ranged between 1 and 17 ms^{-1}. The AHFO measurements are compared to sonic anemometer measurements and show a high ~~overall correlation (0.94~~coefficient of determination (0.98-0.99). Both the precision and accuracy of the AHFO measurements were also greater than 95% for all conditions. We conclude that the AHFO has potential to measure wind speed and we present a method to help for choosing the heating settings of AHFO. AHFO allows for characterization of spatially varying fields of mean wind. In the future, the technique could be combined with conventional Distributed Temperature Sensing (DTS) for turbulent heat flux estimation in micrometeorological/hydrological applications.

1 Introduction

This work presents the results of a wind tunnel study designed to test the novel Actively Heated Fiber-Optic (AHFO) (Sayde et al. (2015)) wind speed measurement technique in controlled airflow conditions. The primary aims of the experiment were to assess the directional sensitivity and signal-to-noise ratio of AHFO.

Wind speed is most commonly observed using in-situ point measurement techniques. As a result, the spatial distribution of field observations is limited. While it is possible to obtain distributed wind speed observations with remote sensing (e.g., Goodberlet et al. (1989); Bentamy et al. (2003)), the spatial resolution is too low for many micrometeorological applications.

Many field experiments assume Taylor's frozen flow hypothesis (Taylor (1938)) in order to estimate fluxes with similarity theory (e.g., Higgins et al. (2009); Kelly et al. (2009); Bou-Zeid et al. (2010); Patton et al. (2011)). However, similarity theory only holds for idealized homogeneous/stationary conditions, which are rarely met in practice, resulting in a model containing strong assumptions, which often leads to significant errors (Ha et al. (2007); Higgins et al. (2012); Thomas et al. (2012)). In real, non-idealized situations, even slight surface heterogeneities can lead to dramatic impacts on the spatial structure of the flow in the surface boundary layer. Further, even if perfect surface homogeneity was possible, other atmospheric (surface) conditions are often nonstationary as well (Holtslag et al. (2013)).

In the past decade, a new way to obtain spatial distributed measurements was introduced into environmental studies. High spatial resolution measurements could be used to check underlying assumptions and would reduce the need for such assumptions in real-world cases. Distributed Temperature Sensing (DTS) technology measures temperature at high temporal and spatial resolution over distances of up to several kilometers by using Fiber Optic (FO) cables as sensors (Selker et al. (2006a); Selker et al. (2006b); Tyler et al. (2009)). High-end DTS can measure the temperature at a 1-s and 0.3-m resolution (Sayde et al. (2014)). The ability to report temperature at such high resolution has proven useful in many environmental studies (Selker et al. (2006a); Selker et al. (2006b); Tyler et al. (2008); Tyler et al. (2009); Steele-Dunne et al. (2010)), including atmospheric experiments (Keller et al. (2011); Petrides et al. (2011); Schilperoort et al. (2018); Higgins et al. (2018); Izett et al. (2019)). It has also been shown that it is possible to observe air temperature and thermal structure of near-surface turbulence with DTS (Thomas et al. (2012); Euser et al. (2014); Zeeman et al. (2015), Jong et al. (2015)).

Recently, Sayde et al. (2015) introduced the AHFO technique where they aimed to use DTS to measure wind speed. The underlying concept of the proposed method is similar to that of a hotwire anemometer; however, instead of single point measurements, AFHO enables distributed measurements to be made at high spatial resolution. Instead of only passively measuring the temperature in the fiber (as is done with DTS), one segment of the cable is actively heated. The heated segment is positioned parallel to the unheated reference segment, with a small separation, in our case 0.1 m. The temperature difference between the heated and reference segment is measured, i.e., the heated fiber and the air temperature. The temperature difference between the cables depends on the energy input as well as on the wind speed of the ambient air, which determines the magnitude of the lateral heat exchange, through convective heat loss. By setting up an energy balance for the heated cable, one can estimate the magnitude of this convective heat transport, which leads to an estimate of the wind speed.

Results from a field study by Sayde et al. (2015) demonstrated promising performance of the AHFO technique, but they recommended further tests on two aspects to be performed in controlled airflow conditions. First, the heat transfer model assumes a flow normal to the axis of the fiber. Hence, non-normal angles of attack need to be accounted for by using directional sensitivity equations. Following the recommendations of Sayde et al. (2015) we tested different directional sensitivity equations from hotwire anemometry (Webster (1962); Hinze (1975); Perry (1982); Adrian et al. (1984)) in the controlled setting of our experiment. Second, Sayde et al. (2015) highlight the importance of a sufficient signal-to-noise ratio when conducting

measurements. They show that the temperature difference between the heated and reference segments gives a good estimate for this ratio. The influence of the directional sensitivity and the signal-to-noise ratio on the measurement accuracy and precision is investigated and the results are used to propose a method to estimate the precision for future experiments with AHFO, hence our work will improve the possibilities for successful application of AHFO in future field experiments.

Finally, in the future it will be interesting to perform outdoor tests with AHFO, for both micrometeorological and hydrological applications, as AHFO gives a lot of insights in spatial varying wind fields. AHFO can be especially interesting in non-homogenous field sites, like forests, which are already studied with other DTS applications (Schilperoort et al. (2018)). Moreover, the ability to measure spatial varying wind fields can be useful for estimating sensible heat fluxes in a variety of atmosphere-vegetation-soil continuums.

An overview of the experimental setup is presented in Section 2, with the accuracy and precision of the AHFO experiments presented in Section 3. In Section 3.4, a method for estimating the precision of AHFO experiments is introduced, followed by a short note on future studies.

2 Experimental Set-Up and Methods

2.1 DTS and Signal-to-Noise ratio analysis

Based on the backscattered signal of a laser pulse inside fiber optic cables, a Distributed Temperature Sensing (DTS) machine measures temperature along a complete fiber optic cable (Selker et al. (2006a); Selker et al. (2006b)). A main source of noise in DTS data is white noise induced by the statistical variability in photon count from backscatter (optical shot noise). The white noise can be reduced by averaging over multiple measurements in either space or time, assuming the observed temperature is/stays (relatively) constant (van de Giesen et al. (2012)).

A sufficiently high signal-to-noise ratio is essential for measurement precision with DTS. In Sayde et al. (2015) it is shown that the signal-to-noise ratio can be described as: $(T_s - T_f)/T_{error}$, where T_s and T_f are the temperature (in K) of the heated cable segment and (unheated) reference segment (i.e., air temperature). Hence the signal-to-noise ratio is related to the ΔT (= $T_s - T_f$) and the measurement error of the DTS, T_{error} (~~in this study at a 1-s sample resolution~~defined by the machine specifications). A large ΔT is obviously desirable, however, ΔT cannot be increased infinitely. The power controller can only deliver a limited amount of power to heat the FO cable, which is especially relevant for the heating of long lengths of FO cable (i.e. several hundreds of meters of FO cable). Additionally larger temperature differences can cause that other ways of transferring energy (e.g., free convection, radiation and diffusion) can become more dominant~~/important~~. The effect of ΔT is investigated by using three temperature differences during the experiment. The effect of the signal-to-noise ratio is quantified, and an equation to estimate the precision is presented. The measurement precision is an indication of the variability of wind speed measurements (e.g., RMSD), as opposed to accuracy which describes a systematic measurement error for which can be compensated (in our case expressed by the bias).

2.2 Determination of Wind Speed

2.2.1 Original determination of Wind Speed by Sayde et al. (2015)

An energy balance is used to quantify the heat dissipation from the heated section, and therefore estimate the wind speed with DTS. The convective cooling can be converted to wind speed, because it is a function of wind speed and the temperature difference between the heated and unheated segments. The full energy balance (in W) for a cable segment volume of length, B, is given by Sayde et al. (2015), and schematically shown in Figure 1:

$$c_s \rho_v V \frac{\mathrm{d}T_s}{\mathrm{d}t} = P_s B + (\bar{S}_b + \bar{S}_d + \alpha_s \bar{S}_t)(1-\alpha_f) 2r\pi B + (\bar{L}_\downarrow + \bar{L}_\uparrow)\epsilon 2r\pi B - \epsilon\sigma T_s^4 2r\pi B - h(T_s - T_f)2r\pi B \quad (1)$$

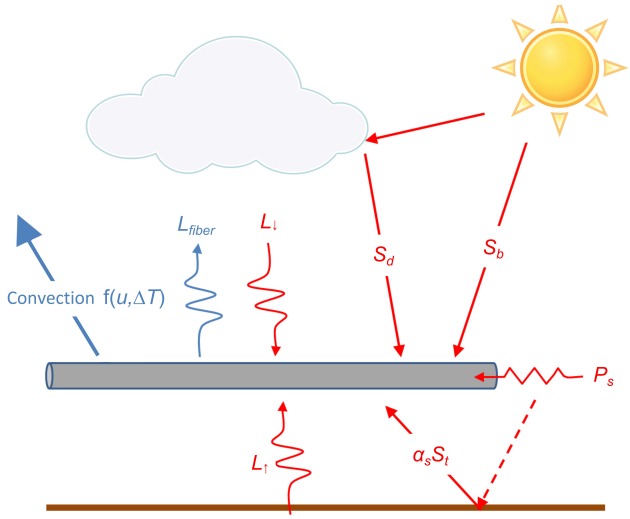

Figure 1. Schematization of the energy balance, based on Sayde et al. (2015)

Where, r is the radius of the cable ($6.7 \cdot 10^{-4}$ m in our setup); V is the volume of the cable segment ($\pi r^2 B$, in m^3), c_s is the specific heat capacity of the FO cable (502 $Jkg^{-1}K^{-1}$) and ρ_v is the FO cable density (800 kgm^{-3}). P_s is the heating rate per meter of cable (in Wm^{-1}); and B is the length of a cable segment (in m). $\bar{S}_b, \bar{S}_d$ and $\alpha_s \bar{S}_t$ (in Wm^{-2}) are the mean direct, diffuse and reflected short wave radiation fluxes, respectively, with α_s being the surface albedo of the ground; and α_f is the FO cable optic surface albedo. $\bar{L}_\downarrow + \bar{L}_\uparrow$ (in Wm^{-2}) are the average downward and upward longwave radiation fluxes, respectively; and ϵ is the FO cable surface emissivity. Based on the kind of stainless steel, emissivity values can range from 0.3 to 0.7 (Baldwin and Lovell-Smith (1992)); however, we assume a value of 0.5 (Madhusudana (2000)). σ is the Stefan-Boltzmann constant, $5.67 \cdot 10^{-8}$ (Wm^{-2} K^{-4}); and $\epsilon\sigma T_s^4$ is the outgoing longwave radiation of the fiber, i.e., L_{fiber}; h is the convective heat transfer coefficient ($Wm^{-2}K^{-1}$).

Simplification

The energy balance is simplified, by dividing Eq. 1 by $2r\pi B$, which is equal to the surface area of the FO cable. The energy balance now no longer depends on B, meaning the length of FO cable segment does not need to be defined. The proposed final energy balance by Sayde et al. (2015) is as follows and in Wm^{-2}:

$$\frac{c_s \rho r}{2}\frac{\mathrm{d}T_s}{\mathrm{d}t} = \frac{P_s}{2\pi r} + (\bar{S}_b + \bar{S}_d + \alpha_s \bar{S}_t)(1-\alpha_f) + (\bar{L}_\downarrow + \bar{L}_\uparrow)\epsilon - \epsilon\sigma T_s^4 - h(T_s - T_f) \tag{2}$$

where, ρ is the FO cable density per meter of cable segment: 4.5 x 10^{-3} kgm^{-1}.

Convective heat transfer coefficient

The convective heat transfer coefficient h ($Wm^{-2}K^{-1}$) can by means of the dimensionless Nusselt (Nu), Prandtl (Pr), and Reynolds (Re) numbers be expressed as function of the wind speed, $h = f(u_n)$. The Nusselt number is the ratio between the advective and conductive heat transfer, where the Nusselt number can be written as follows (Žukauskas (1972)):

$$\mathrm{Nu} = \frac{h d_s}{K_a} = C\mathrm{Re}^m \mathrm{Pr}^n \left(\frac{\mathrm{Pr}}{\mathrm{Pr}_s}\right)^{\frac{1}{4}} \tag{3}$$

with,

$$\mathrm{Re} = \frac{u_n d_s}{\upsilon_a} \tag{4}$$

d_s is the fibers characteristic length ($2r$); K_a is the thermal conductivity of air and υ_a the kinematic viscosity of air, respectively 0.0255 $Wm^{-1}K^{-1}$ and 1.5 x 10^{-5} m^2s^{-1} (Tsilingiris (2008)). K_a and υ_a are assumed to be constant, due to the controlled conditions in the wind tunnel, but in field experiments this should be included as a variable, as K_a and υ_a are temperature and relative humidity depend (Tsilingiris (2008)). C, m and n are empirical constants related to forced advection of heat by air movement. In Sayde et al. (2015), C, m and n values of 0.51, 0.5 and 0.37 are set, based on (Žukauskas (1972)). Pr is the Prandtl number and can be seen as the ratio between kinematic viscosity and thermal diffusivity, which, we assume Pr to be constant (0.72) for our range of temperatures (12-35 K), as in Tsilingiris (2008), with Pr_s (the Prandtl number for the heated fiber segment), assumed to be the same as Pr, due to the small temperature differences (max. 6 K). Lastly, Re is the Reynolds number which is used to determine the flow regime of the air along the fiber segments, i.e., Re expresses if the flow regime is laminar or turbulent. Combining Eq. 3-4 yields:

$$h = Cd^{m-1}\mathrm{Pr}^n \left(\frac{\mathrm{Pr}}{\mathrm{Pr}_s}\right)^{\frac{1}{4}} K_a \upsilon_a^{-m} u_n^m \tag{5}$$

The determination of the Nusselt number (Eq. 3) is only valid in the following ranges of Re (40-1000) and Pr (0.7-500). Re can be a limitation for higher wind speeds, especially when the diameter of the fiber is large, in our case wind speeds higher

than approximately 11 ms^{-1} would be out of range. In the derivation of the energy balance (1), there is assumed to be no free convection, induced by heating of the air close to the cable, and no conduction of heat in the axial direction of the FO cable. It is also assumed there is no radiative exchange between objects close and parallel to the heated fiber, i.e., dispersion of heat from the heated cable to the reference cable is assumed to be negligible. Furthermore, a flow directed normal to the axis of FO cable is assumed by the proposed energy balance, i.e., for flow directed in a different angle, compensation is necessary to accurately estimate the wind speed.

2.2.2 Revised simplified determination of Wind Speed

Due to the setup inside the wind tunnel, as opposed to outdoor conditions, some simplifications can be made. The short wave radiation can be neglected because it is an indoor experiment (no sunlight). Furthermore, we assume that there is a uniform temperature inside the wind tunnel, due to the enclosed conditions. This means the incoming radiation is dependent on the air temperature, T_f. Assuming incoming ($\bar{L}_\downarrow + \bar{L}_\uparrow$) to be black body radiation (i.e., $L_{in} = \sigma T_s^4$), the net longwave radiation loss for the fiber can be simplified accordingly by merging the incoming longwave and outgoing longwave radiation as:

$$(\bar{L}_\downarrow + \bar{L}_\uparrow)\epsilon - \epsilon\sigma T_s^4 \approx -\epsilon\sigma(T_s^4 - T_f^4) \tag{6}$$

One more additional change is made, based on our results obtained during testing of the performance of the AHFO technique. In processing of the obtained wind tunnel data it was found that by using the calculation of the Nusselt number from Žukauskas (1972), Eq. 3, a $\sim 20\%$ additional bias in calculating the wind speed was created. By using a more recent version for calculating the empirical Nusselt number (Cengel and Ghajar (2014)), the bias in our study is reduced to $\sim 5\%$ Therefore, Eq. 7 is proposed to calculate the Nusselt number, where the constants C, m and n are still used; however, with the values from Table 7-1 ($C = 0.683, m = 0.466$ and $n = 1/3$) in Cengel and Ghajar (2014), rather than those in Žukauskas (1972). Next to the improved fit, the range of Re over which the equation is valid is much wider (40-4000 compared with 40-1000), and therefore more applicable in future AHFO experiments.

$$\mathrm{Nu} = C\mathrm{Re}^m\mathrm{Pr}^n = 0.683\mathrm{Re}^{0.466}\mathrm{Pr}^{1/3} \tag{7}$$

Consequently, the expression of h changes as well.

$$h = Cd^{m-1}\mathrm{Pr}^n K_a \upsilon_a^{-m} u_n^m \tag{8}$$

With the long- and short-wave radiation simplifications, the energy balance becomes:

$$\frac{c_s \rho r}{2}\frac{\mathrm{d}T_s}{\mathrm{d}t} = \frac{P_s}{2\pi r} - \epsilon\sigma(T_s^4 - T_f^4) - h(T_s - T_f) \tag{9}$$

By substituting the expression for h (Eq. 8), we can rearrange Eq. 9 to obtain an expression for wind speed. Eq. 10 will be used to estimate the wind speed (u_N) in our wind tunnel study.

$$u_N = \left(\frac{0.5 P_s \pi^{-1} r^{-1} - \epsilon\sigma(T_s^4 - T_f^4) - 0.5 c_p \rho r \frac{\mathrm{d}T_s}{\mathrm{d}t}}{C d^{m-1} \mathrm{Pr}^n K_a \upsilon_a^{-m} (T_s - T_f)} \right)^{1/m} \tag{10}$$

2.3 Wind tunnel experiments

We conducted a series of experiments under tightly controlled airflow conditions to improve the applicability of AHFO in experimental (field) research and to study the directional sensitivity and influence of the signal-to-noise ratio. The experiments presented were performed in a wind tunnel at Oregon State University. This wind tunnel has a closed circuit, which means the air inside is recycled. The test section of the wind tunnel has a cross-section (height by width) of 1.23 by 1.52 m, and an undisturbed horizontal section of roughly 5 to 6 m which may be used for probing. During the experiment two segments of one cable (which encloses the FO cores) were placed 8 cm apart: one heated and one reference segment. For validation, an independent sonic anemometer (IRGASON+EC100 and CR3000, Campbell Scientific, Logan, UT,USA) was placed approximately 0.2 m downwind of the fibers, which measures the wind speed in 3 directions at 10 Hz. As the FO cables are very thin, it is assumed that these do not significantly disturb the measurement of the sonic volume (particularly at larger averaging times). All equipment was mounted using custom-designed support material.

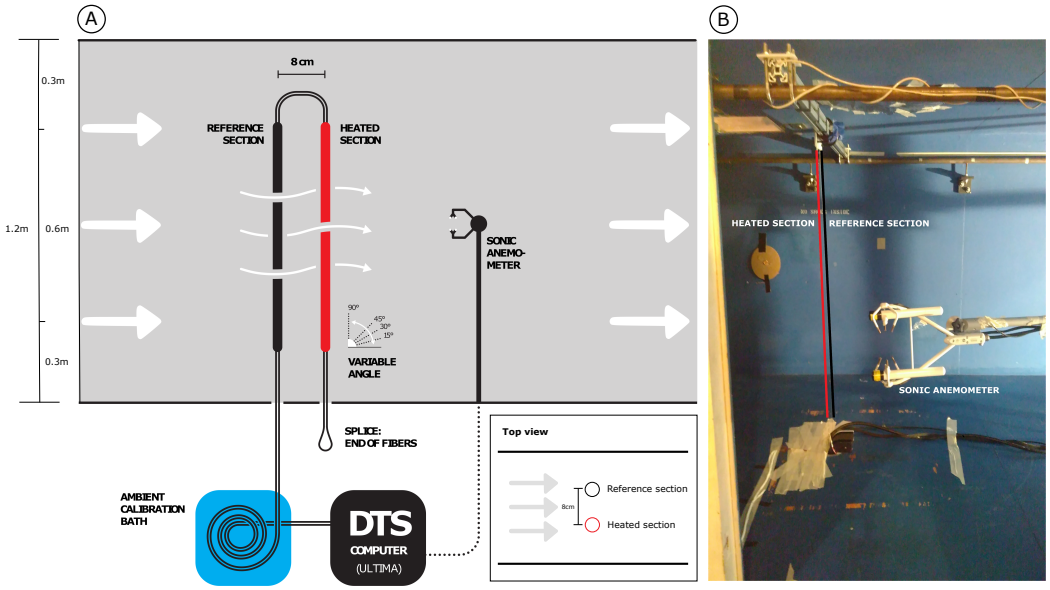

Figure 2. a) Schematic of the wind tunnel setup and b) photograph of the experimental setup in the wind tunnel.

The cable (AFL, Spartanburg, SC, USA) mounted in the wind tunnel consisted of a 1.34 mm outer diameter stainless steel casing that enclosed four multi-mode FO cores with a diameter of 250 µm (Figure A1). The electrical resistance per meter of stainless steel casing (R_s) is 1.67 (Ωm^{-1}) and is constant along the length, where for the length of a cable segment (B, (m)), $R = R_s B$, where R (Ω) is the total resistance of a cable segment. Similary the heating rate is defined as $P_s = I^2 R_s$ (Wm^{-1}) per meter of cable segment, where I (A) is the eletrical current. Only two FO cores were used and these were spliced at the end of the cable to create a duplexed FO core, which results in double measurements for each measuring point along the FO cable, using a single-ended configuration (Hausner et al., 2011). The FO cores were connected to a Silixa Ultima DTS machine (Ultima S, 2 km range, Silixa, London, UK) outside the wind tunnel.

One cable segment was heated by connecting the stainless steel casing to a power controller (MicroFUSION uF1HXTA0-32-P1000-F040) by 12 AWG (copper) cables (3.31 mm^2), to heat the cable in a controlled way.

For calibration and validation of the DTS data, approximately 6 m of the FO cables was placed in a well-mixed ambient bath to calibrate the DTS temperature according to the method described by Hausner et al. (2011). The temperature was verified with one probe (RBRsolo^2 T, RBR Ltd., Ottawa, Ontario, Canada). A circulating aquarium pump was placed inside the bath, to prevent stratification.

In field experiments the wind speed and direction will vary, therefore different angles of attack and wind speeds are tested. Additionally different heating rates are used to quantify the importance of the signal-to-noise ratio. The following settings are used:

- **Angle of attack**: The cable was mounted at four different angles in the wind tunnel, resulting in different angles of attack to mean flow direction, in order to gain more insights into directional sensitivity. In Figure 2b the 90° set-up is visible, however the cable was also mounted at a 45°, 30° and 15° angle, with respect to the floor of the wind tunnel (see: Figure 2a, inset). During all set-ups, the lower part of the FO cable was fixed to the opening in the bottom of the wind tunnel, while the upper end was attached to an extruded aluminum bar that was moved over the fixed horizontal bars, to achieve the desired cable angles.

- **Wind speed**: To test the performance for a range of wind speeds, ten different wind speeds were tested at every angle: 1, 3, 5, 7, 9, 11, 13, 15, 16 and 17 ms^{-1}. The AHFO wind speed measurements can be adjusted by comparing the AHFO wind speed to a reference sonic anemometer. The wind speed in the wind tunnel was fixed at a constant value to create a stable, non-turbulent, steady state flow (Appendix C).

- **Heating rate**: The magnitude of the current needed to create a given temperature difference is dependent on the cable resistance and the wind speed, therefore the current is adjusted for each individual experiment. The current was fixed to create a temperature difference (ΔT) of 2, 4 and 6 K between the heated and reference cable. Heating rates varied from 0.5-10 Wm^{-1} during our setup.

In total, 120 (4 x 10 x 3) trials were conducted with the different parameters, each with a minimum duration of 10 minutes.

Temperatures along the FO cable were sampled at 0.125 m resolution with a sampling rate of 1 Hz. Splices between ends of fiber optic cables are known to create an additional loss in signal, i.e., local higher attenuation (Tyler et al. (2009); van de

Giesen et al. (2012)), this loss is normally independent of the direction. However, in processing of the raw DTS data it was found that the loss over the splice was not the same in both directions. Due to this asymmetrical structure of the splice loss, only the data of one channel was used to ensure the quality of the results, as this channel showed a regular splice loss.

For each angle of attack only the 5 temperatures differences ($\times 2$ because of ~~duplexing~~duplexed FO core) from the middle of the wind tunnel are used, to prevent using AHFO wind speed measurements with side/boundary effects. We investigated the consequences of extending the spatial range and found there is limited difference between these measurements (see Table D1). During this extended spatial range analysis we found out part of the 90° data ~~of the duplexed cable~~ contained additional noise which decreased the accuracy, and therefore we decided to take only 5×1 temperature differences for the 90° calculations. Potential reasons for this additional noise could be the sharper bend for the 90° setup, also the FO cable is shorter for the 90° setup (due to the design of the setup), what means the fixations are closer to the middle of the cable causing local disturbances on the temperature measurements.

In our study we use the advantage of averaging over time and space, to reduce (white) noise in the DTS measurements (van de Giesen et al. (2012); Selker et al. (2006b)). For clarity we therefore introduce three parameters: n_{time}, n_{space} and n, where n_{time} is the amount of measurements averaged over time and n_{space} is the amount of measurements averaged over space and n the total amount of measurements over time and space and can be expressed as: $n = n_{time} \times n_{space}$. In the machine specifications it is given that the sample resolution is $x_{sample} = 0.125$m~~, but the~~. The highest actual spatial resolution is 0.3m, indicating ~~and~~ a $n_{space} \geq 2$, according to the 10-90% rule as described in Tyler et al. (2009). In this paper we will first work with $n_{space} = 10$ and finally we will propose an equation to predict the precision (See later Eq. 21) which is a function of n_{space} and n_{time}. ~~This is done, because we want to estimate~~ We first use $n_{space} = 10$, because for deriving the precision prediction an unique constant (C_{DTS}) is necessary. C_{DTS} is independent of the DTS machine and ~~the settings, which~~ settings, and is expected to be more ~~representative~~ accurate if the amount of (white) noise is reduced by averaging.

2.4 Directional sensitivity analysis

Equation 10 is derived for flows normal to axis of the cable (as in Figure 2b). However, in reality the wind will not always have a 90° angle compared to the axis of the cable, especially in outside atmospheric experiments. For angles smaller than 90° the wind speed will be underestimated, as the convective heat transfer is less efficient. While Sayde et al. (2015) adjusted the wind speed of the sonic anemometer using a geometric correction from hotwire anemometry (e.g., Adrian et al. (1984)), we adjusted the measured DTS windspeed u_N (eq. 10) to compare both wind speeds:

$$u_{DTS} = \sqrt{\frac{u_N^2}{\cos^2(\varphi - 90°) + k_{ds}^2 \sin^2(\varphi - 90°)}} \tag{11}$$

k_{ds} is the directional sensitivity and φ is the angle of attack of the wind with respect to the axis of the cable, ranging from 0° to 90°.

2.5 Accuracy and precision definition

The perfomance of our AHFO measurements will be assed by looking at the accuracy and precision. The accuracy (σ_a) is defined by the normalized difference of the AHFO and sonic anemometer wind speed measurements, Eq. 12.

$$\sigma_a(j) = \frac{\bar{u}_{DTS}(j) - \bar{u}_{sonic}(j)}{\bar{u}_{sonic}(j)} \tag{12}$$

Where j is a specific wind speed setting, where $j = 1, 3, 5, 7, 9, 11, 13, 15, 16, 17$ ms^{-1}. And $\bar{u}$ is the average of all indivual measurements (i) for a given wind speed setting.

The precision (σ_p) is defined by the normalized RMSD between the AHFO and sonic anemometer wind speed measurements, 13.

$$\sigma_p(j) = \frac{\text{RMSD}}{\bar{u}_{sonic}(j)} = \frac{\sqrt{\sum \left(\left(u_{sonic}(i,j) - \bar{u}_{sonic}(j) \right) - \left(u_{DTS}(i,j) - \bar{u}_{DTS}(j) \right) \right)^2 \frac{1}{n(i)}}}{\bar{u}_{sonic}(j)} \tag{13}$$

3 Results and Discussion

3.1 Proposed directional sensitivity equation

During analysis of the wind tunnel data it was found that Eq. 11 was not giving satisfying results (e.g., a 22% bias between the 90° and 15° angle). In Adrian et al. (1984) it is shown that in hotwire anemometry a variety of theoretical and empirical formulas have been proposed in the past, in order to account for directional sensitivity. Alternatively, using the formula suggested by Bruun (1971) gives more satisfying results, diminishing the bias between the 90° and 15° angle to only ~~4%~~a few percent. This is shown in the boxplot of Figure 3.

Therefore, Eq. 14 is used to account for directional sensitivity in our study, with the scaling exponent, m_1, able to be optimized during calibration of the AHFO measurements. The value for m_1 obtained during calibration of our set up was 1.05.

$$u_{DTS} = \frac{u_N}{\cos(\varphi - 90°)^{m_1}} \tag{14}$$

3.2 Accuracy and precision

In Figure 3b the AHFO wind speed measurements are compared to the velocity measured with the sonic anemometer. The comparison for all angles can be found in Figures B1 and B2. The wind speeds measured with AHFO are calculated using 10 temperature differences (duplex setup with 2×5 heated and reference measurements), i.e., for the 90°setup this is equivalent to a height of $\sim$ 0.675 m in the wind tunnel.

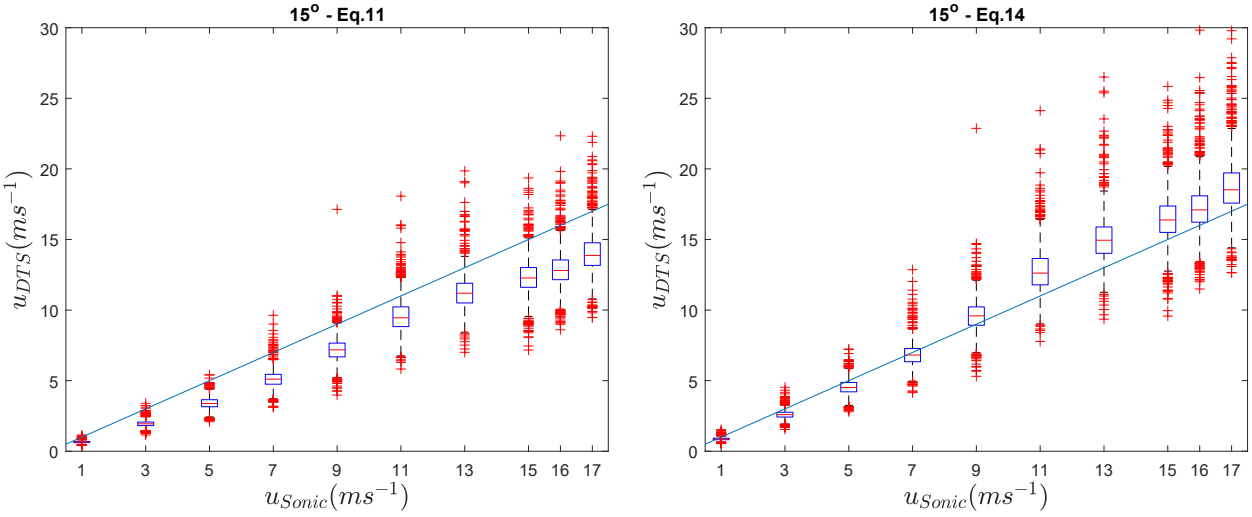

Figure 3. Directional sensitivity shown in boxplots for 15° angle, original Eq. 11 (a) and proposed Eq. 14 (b). The line represents the 1:1-line.

Figure B1 shows the sample rate DTS data against the 1-s average sonic anemometer data, for the four different angles of attack. Figure B2 shows the same ~~dataset, but temporally averaged over 30-s, and~~ data set, but then combined for all angles, for a 1-s and temporally averaged 30-s resolution. A clear improvement of the precision is visible when temporal averaging is performed. Even though the directional sensitivity formula is not yet fully calibrated, the bias is negligible, with ~~coefficients of determination ranging from 0.94~~a coefficients of determinations ranging from 0.98-0.99, with a slope ranging from 0.92 to 1.15 and a intercept ranging from -0.71-0.6. Finally, as expected, the wind speed measurement are less accurate when the wind speed angle is smaller.

To get more insight in the quality of the results, a dimensionless analysis is performed. In Figure 4, the non-dimensional wind speed accuracy for the whole wind tunnel experiment is shown. For all combinations (120 individual cases of varying wind speed (j), angle and ΔT), the accuracy is calculated according to Eq. 12. σ_a is a dependent on the averaging time, which is defined as $n_{time} = t_{avg}/t_{sample}$, where t_{avg} can only be a integer which is a multiple of t_{sample}. σ_a is also a dependent on spatial averaging, which is defined as $n_{space} = x_{avg}/x_{sample}$, where x_{avg} can only be a integer which is a multiple of x_{sample}. In Figure 4 the accuracy is averaged over all wind speeds for each ΔT and angle combination, with $n_{space} = 10$ and n_{time} varying from 1 to 30, resulting in 12 values for each time resolution.

For the data set, the maximum σ_a is $\pm$ ~~3%~~0.03, which is promising for future applications. The $\Delta T = 6K$ should be the best performing heating setting, however this is not always the case and there ~~is~~ are fluctuations between the heating settings, which could be due to neglecting small energy losses, like free convection due to heating of air close to the heated cable (Sayde et al. (2015)), which is temperature dependent. With such an energy loss included, the bias of each angle might change. Nevertheless, the bias is fairly constant after 5-s with increasing averaging time, which means ~~extensive calibration~~

further analysis can probably increase the accuracy. The change in bias from 1s to 5-s is due to the precision of our AHFO measurements, which increases with averaging over time and is higher for a greater ΔT.

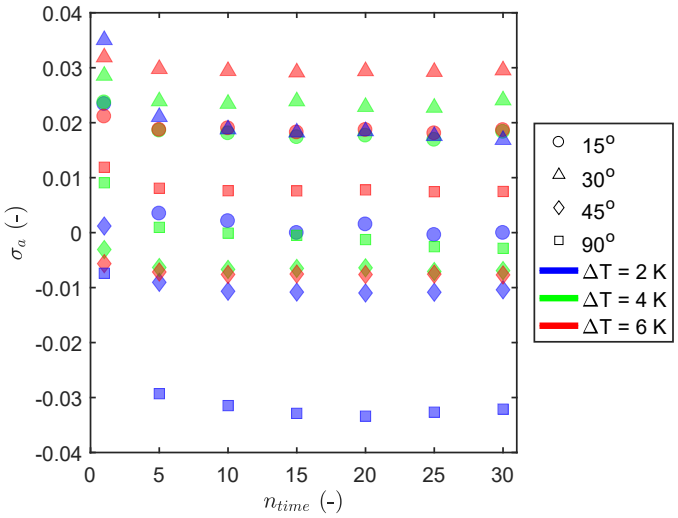

Figure 4. Bias in AHFO wind speed as a function of averaging period for different angles of attack, and different fiber heating. With $n_{space} = 10$.

While the accuracy (bias) remains fairly constant over the averaging period, the relative precision, σ_p improves significantly (Fig. 5). The precision is calculated for all 120 ΔT, angle and wind speed combinations (where $j = 1, 3, 5, 7, 9, 11, 13, 15, 16, 17$ ms^{-1}), using Eq. 13. ~~Similar to the accuracy, the precision, σ_p, is dependent on the averaging time and spatial averaging.~~

~~While calculating the precision of~~ For the calculation of the precision u_{DTS}, we considered the natural variability of the wind~~is excluded, by assuming~~. We assumed that this natural variability is measured by the sonic anemometer ~~is able to capture the natural variability and assuming the sonic anemometer measurements have a negligible instrument variability in comparison to the AHFO measurements. As a result,~~ measurements and we assume that this per definition is smaller than the variability of the DTS machine u_{DTS} estimates. After applying Eq. 13 the variability of the DTS machine u_{DTS} ~~estimates~~ are obtained. For each of the 120 combinations, $\bar{u}_{sonic}(j)$ and $\bar{u}_{DTS}(j)$ are the average wind speeds for a j. $u_{sonic}(i,j)$ and $u_{DTS}(i,j)$ are single measurements for a j.

~~To be able to present the precision clearly, the precision is averaged over wind speed for all~~ The precision was averaged over all wind speeds for each ΔT and angle combinations in Figure 5, ~~with n_{space}=10 and n_{time} varying from 1 to 30, resulting in 12 values for each time resolution~~which is justified because σ_p is normalized by the mean wind speed, hence any linear dependency should be removed.

The precision improves to a σ_p less than ~~5%~~ 0.05 by averaging over time. Improvement by averaging is expected due to the reduction of noise (van de Giesen et al. (2012)). As mentioned, the main source of noise in DTS data is white noise, this explains the visible improvement of the precision by $\frac{1}{\sqrt{n}}$, as signal averaging is applied, where n is the amount of measurements (Selker

et al. (2006b); Kaiser and Knight (1979)). Hence, in this paper n is expressed as $n_{space} \times n_{time}$, the amount of measurements in the time and space domain.

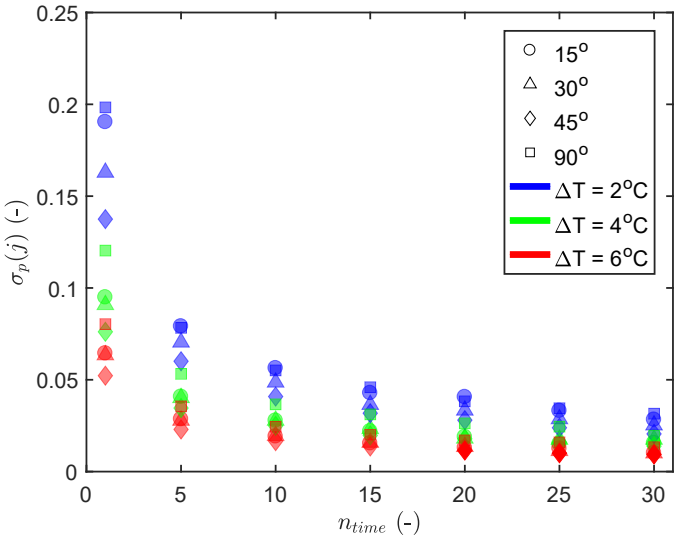

Figure 5. Precision of the AHFO wind speed measurements as a function of averaging period. With $n_{space} = 10$.

3.3 Normalized precision independent of sampling settings

In order to remove the influence of different settings (such as the choice of ΔT) and determine a general prediction of precision in future experiments, we normalize the precision. First, the precision is normalized to ΔT (Figure 6a), by multiplying Eq. 13 by $\frac{\Delta T}{T_{error}}$, which can be written as Eq. 15.

$$\sigma_p(j, \Delta T) = \sigma_p(j) \cdot \frac{\Delta T}{T_{error}} \tag{15}$$

As a results, $\frac{1}{\sqrt{n}}$ dependence becomes even more clear, as shown by the black solid line showing $\frac{\bar{\sigma}_p}{\sqrt{n_{time}}} \times \frac{\Delta T}{T_{error}}$, where $\bar{\sigma}_p$ is the average of Eq.13, with $n_{space} = 10$ and n_{time}=1. Second, the precision is also normalized to the $\frac{1}{\sqrt{n}}$ behavior, by multiplying Eq. 15 by $\sqrt{\frac{t_{avg}}{t_{sample}}}$, resulting in Eq. 16.

$$\sigma_p(j, \Delta T, n_{time}) = \sigma_p(j) \cdot \frac{\Delta T}{T_{error}} \sqrt{\frac{t_{avg}}{t_{sample}}} \tag{16}$$

T_{error} and t_{sample} are given constants which depend on the performance of the DTS, in this case $T_{error} = 0.25$ K and $t_{sample} = 1$-s, both according to the factory specifications. It appears that the precision by taking the average can be condensed

in one number, 1.6, which we denote by the symbol C_{int} (Figure 6b). Intermediate constant C_{int} can be defined as, Eq. 17, with $n_{space} = 10$:

$$C_{int} = \overline{\sigma_p(j) \cdot \frac{\Delta T}{T_{error}} \sqrt{n_{time}}} = 1.6 \tag{17}$$

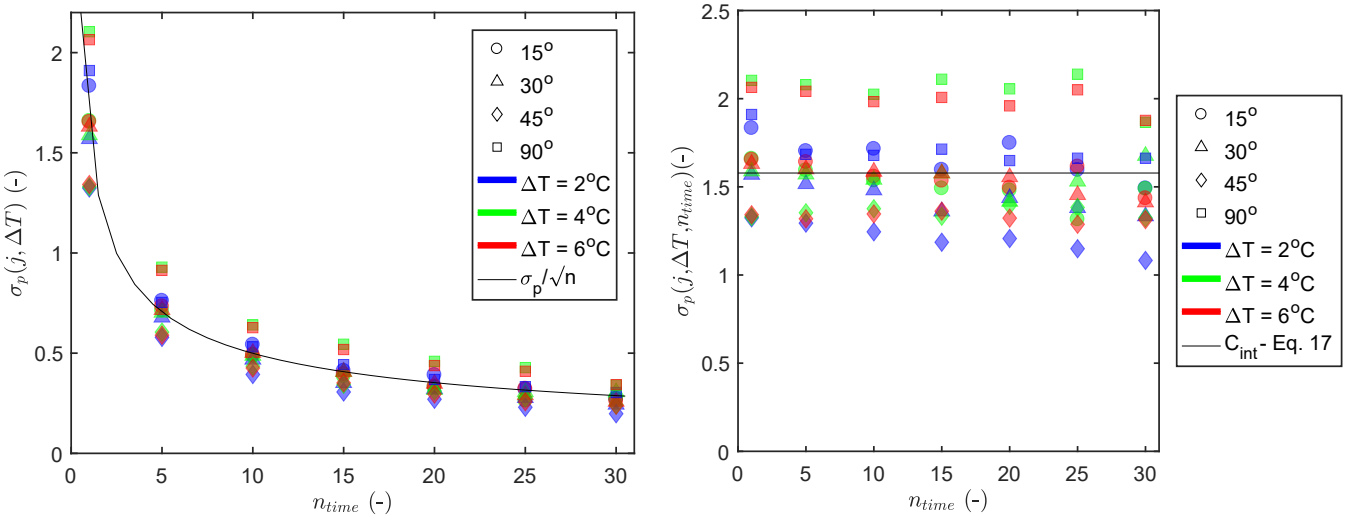

Figure 6. a) Precision of the AHFO wind speed measurements as a function of averaging period, independent of ΔT; and b) Precision of the AHFO wind speed measurements as a function of averaging period. Independent of ΔT and averaging period. With $n_{space} = 10$.

Finally, a final constant for a 1-s and 0.125-m resolution is desired, ~~as this is the sampling resolution and the starting point before any averaging takes place. Doing so , Eq. 21~~ so it can be used for different kinds of DTS machines, also when a DTS machine has different sampling resolutions. ~~Furthermore it is possible to increase the precision of the observation by either averaging over space or time, depending on the scientific research question to be answered with AHFO.~~ By using the shown $\frac{1}{\sqrt{n}}$ dependency, we can convert C_{int} into C_{DTS}, by multiplying C_{int} by $\sqrt{\frac{10}{1}}$, as n_{space} is 10. This results in Eq. 18 with n_{space}=1 and n_{time}=1. C_{DTS} is in our paper on purpose not calculated at once, but derived using C_{int}. As the wind speed in the middle of the wind tunnel can be assumed constant, we expect C_{DTS} to be better by using 5 measurements in the middle of the wind tunnel instead of picking one of these 5.

$$C_{DTS} = \overline{\sigma_p(j) \cdot \frac{\Delta T}{T_{error}} \sqrt{n_{time}}} \cdot \sqrt{n_{space}} = C_{int}\sqrt{10} = 5.0 \tag{18}$$

3.4 Precision prediction

At the start of a new AHFO experiment it is unknown how to make sure the signal-to-noise ratio is sufficient, such that σ_p is small. However, given the result that the increase in precision behaves ~~independent of~~ similar for each ΔT and the averaging time, it is possible to make a prediction for the precision of future work.

In outdoor experiments, the only setting which can be changed is the heating rate, P_s, which is assumed to be fixed at a single value. The idea behind the precision prediction is to guide the choice of a heating rate, such that a preferred precision is achieved for a known dominant wind speed range. As the wind speed outside will vary naturally, ΔT will change accordingly. Therefore, to obtain an expression where P_s is the only unknown, ΔT first needs to be expressed as a function of the wind speed u_n and the heating rate (P_s). This can be done by using Eq. 10. To obtain a first estimate, some assumptions can be made. The numerator of Eq. 10 consists of three terms, of which the first one with heating rate (P_s) is dominant compared to the other ones, namely 10-100 times bigger. When these minor terms are neglected Eq. 10 can be simplified to:

$$u_N = \left(\frac{0.5 P_s \pi^{-1} r^{-1}}{C d^{m-1} \mathrm{Pr}^n K_a \upsilon_a^{-m} (T_s - T_f)} \right)^{1/m} = \left(\frac{A P_s}{B \Delta T} \right)^{1/m} \tag{19}$$

With $A = 0.5\pi^{-1}r^{-1}$, $B = C(d)^{m-1}\mathrm{Pr}^n K_a \upsilon_a^{-m}$ and $\Delta T = T_s - T_f$, resulting in an expression for ΔT as a function of wind speed:

$$\Delta T = \frac{A P_s}{B u_n^m} \tag{20}$$

Knowing this expression of ΔT, Eq. 20 can again be rewritten into Eq. 21, which expresses the precision estimate, with P_s as only parameter which can be changed during an experiment.

$$\sigma_p(j, n_{space}, n_{time}, P_s) = C_{DTS} \frac{B T_{error} u_n^m}{A P_s} \sqrt{\frac{1}{n_{space} \cdot n_{time}}} \tag{21}$$

Where $n_{space} \times n_{time}$ is the number of measurements over which the observed wind speed is averaged, in either space or time domain. By assuming that all constants are known from literature and the set-up, a first estimate of the error can be made for every velocity or heating rate given. If a dominant wind speed range for a new project is known, an associated heating rate can be found, such that the error is sufficiently small.

As an example, Figure 7 shows the estimated precision for our experiment at 1-s ($n_{time} = 1$) and $\sim$ 0.675-m ($n_{space} = 10$) resolution over a range of wind speeds and heating rates. If the diameter of the fiber is different, this is taken into account via term A from Eq. 21, which includes the radius ($d = 2r$). Also, when a DTS machine with a different performance is used, this can be implemented by changing T_{error} accordingly. Of course different applications will demand different space-time averaging windows, depending on the scientific research question to be answered with AHFO, which option is included by $\sqrt{\frac{1}{n_{space} \cdot n_{time}}}$.

In outdoor experiments, the influence of the short and long wave radiation will be present. However, as long as the radiation is the same for the heated and non-heated segment, this does not influence the error estimation, as for the signal-to-noise ratio, ΔT is the most important factor. When the heated and reference fiber are close to each other, which is also needed for properly estimating the wind speed, both fibers will experience a similar contribution of external radiation, such that the overall ΔT will be relatively unaffected by this factor.

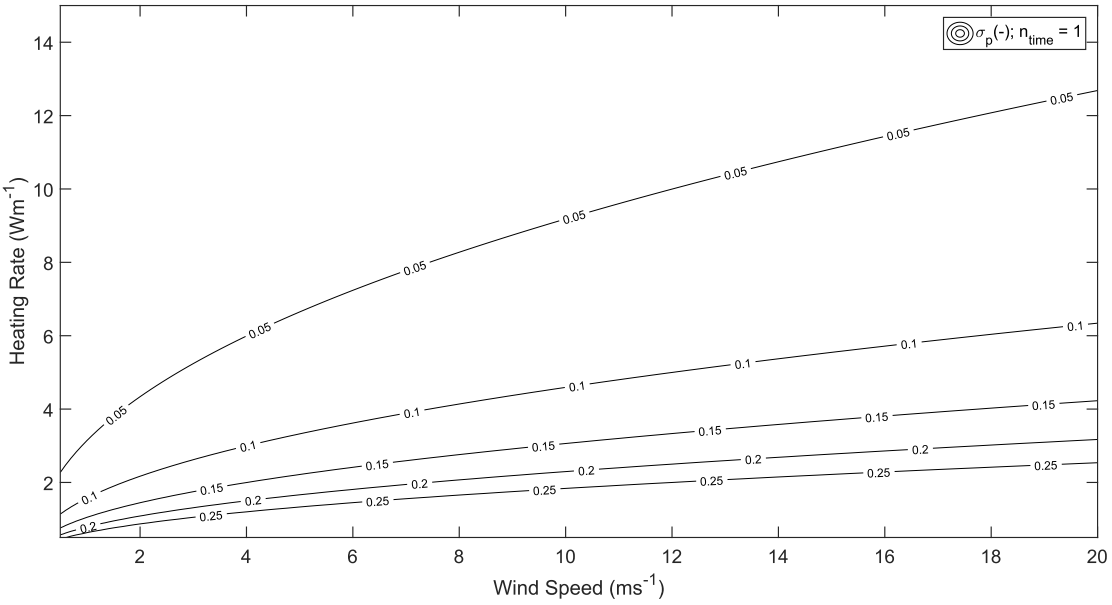

Figure 7. Expected precision (contour lines) for a given heating rate and wind speed as calculated from Eq. 21, with $n_{space} = 10$ and $n_{time} = 1$.

Verification of the precision prediction

For verification purposes the calculated precision (Eq. 13) is combined with the predicted precision (Eq. 21) in Figure 8. As can be seen in Figure 8 we underestimate the precision of the AHFO system using $C_{int} = 1.6$, meaning that better performance can be expected. This difference can be explained by three causes. First, in Figure 6b it is visible that the 90° data is only averaged over 5 data points instead of 10, resulting in a higher C_{int}. Second, we see the effect of ΔT: how higher the heating the less spread in the precision distribution (Figure 5). Third, we neglect the smaller energy terms in Eq. 19, which leads to an increased σ_p. To investigate the sensitivity of using a constant C_{int}, the 98% confidence bounds (two times standard deviation) of C_{int} are determined. It is projected (dotted lines) in Figure 8 that the calculated precision is within the 98% confidence interval of the predicted precision. Concluding, with our prediction equation we can predict all our settings within a 98% confidence interval, showing the general applicability.

3.5 Considerations using AHFO outdoors

The experiments described here were performed in a controlled wind tunnel environment. When performing outdoor AHFO experiments, several factors need to be considered. First of all, during field experiments the relative humidity and temperature might have such a big range that assuming certain parameters (e.g., K_a and υ_a) as constant is not applicable anymore (Tsilingiris (2008)). Furthermore, for small wind speeds (e.g., < 1 ms^{-1}), the neglection of energy losses like free convection

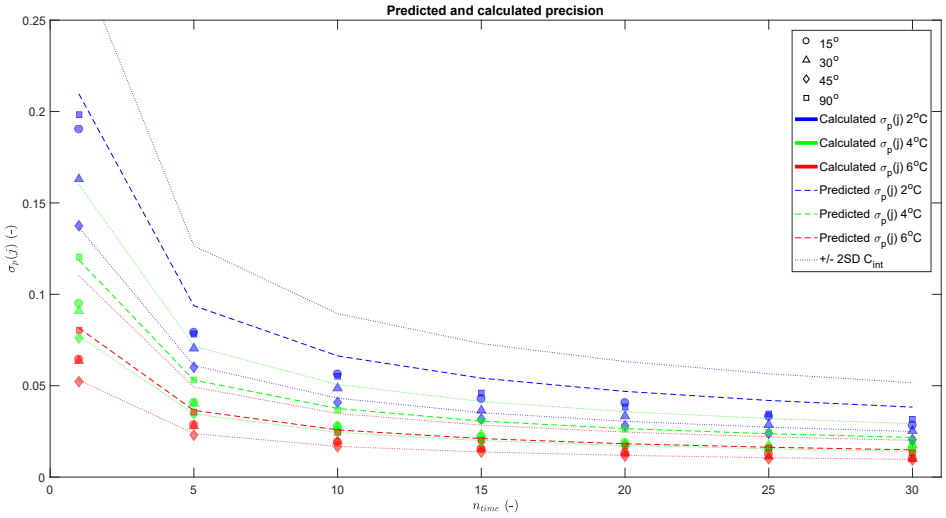

Figure 8. Verification of the precision function (Eq. 21). The predicted precision (dashed lines) is compared with the calculated precision from our experiment (Eq. 13). The dotted lines show the prediction width a $\pm$ 2 standard deviation of C_{int}.

seems not entirely applicable, as this term becomes more dominant in comparison to forced convection. This is confirmed in our study, where it was visible that the response is different between a well ventilated and non-ventilated cable, hence the accuracy is dependent on the wind speed. Although not shown in this paper, it seemed there was no time response difference between a vertical or horizontal mounted heated cable, however by mounting the cable in a horizontal or vertical direction, free convection might influence the temperature measurements as the heated air is moving upward.

Also, the flow in the wind tunnel is laminar and has less turbulence than in outdoor conditions (Appendix C). This is a good setting for calibration of the AHFO method, however in outdoor conditions (small scale) turbulence around the cable is something to take into account. Especially with smaller wind speeds the cooling by turbulence around the cable can be an additional heat loss component, which is not included in the energy balance and therefore could lead to overestimation of the wind speed. Furthermore, one should take into account that wet fibers, due to rain or dew fall, might have an altered heat loss.

It is shown that AHFO can give reliable wind speed measurements, however the precision and accuracy is not as good as with a sonic anemometer. The major addition of AHFO is the possibility to sample the wind speed with a high spatial distribution. It should be taken into account that the time resolution is lower than that of a sonic anemometer and therefore AHFO is less suitable for small scale turbulence, but larger scale turbulence (>1-s; >0.3-m) can potentially be fully captured with a 2D/3D setup with distributed measurements. Despite the high potential resolutions (1-s and 0.3-m) the user should consider to average in either the space or time domain to enhance the precision of the obtained data. The choice for averaging over space or time should be made based on the researched topic.

Finally, when measuring in the field, the use of high quality reference point measurements (e.g., sonic anemometer) is recommended, for example to be able to compensate for possible biases. A sonic anemometer can also be useful to determine

the angle of attack, as this is not (yet) possible with one single fiber. A more complex 3D set-up is necessary to be able to do this with DTS/AHFO (Zeeman et al. (2015)), something which would be interesting to be tested with AHFO in a field experiment.

4 Conclusions

Through a series of controlled wind tunnel experiments, new insights into the accuracy and precision of the newly introduced AHFO wind speed measuring technique were obtained. With high spatial (0.3-m) and temporal (1-s) resolution, the AHFO wind speed measurements agreed very well with the sonic anemometer measurements, with ~~a~~ coefficients of determination ~~ranging from 0.94~~of 0.98-0.99. It is also shown that the AHFO technique has the possibility to measure with a precision and accuracy of 95%. Some additional work is needed, as there still is a small overestimation, which may be caused by neglecting some energy fluxes, such as free convection due to heating of the air close the heated cable. Furthermore, it is possible to optimize the directional sensitivity compensation by extended calibration. Compensating for the directional sensitivity requires ancillary measurement devices in order to measure the angle of attack.

The error prediction equation (Eq. 21) is an important result of this work that will aid in the design of future experiments. This design tool helps with choosing a heating rate for the actively heated fiber in order to be able to create a sufficiently high precision. Based on the prevalent wind speeds of a potential field experiment site, a first estimate of an associated sufficient heating rate can be calculated. Due to the way this design tool is constructed, it can be a good first estimate for all kinds of fibers, DTS precisions, and user preferred spatial and temporal resolutions.

The AHFO technique can reliably measure wind speeds under a range of conditions. The combination of high spatial and temporal resolution with high precision of the technique opens possibilities for outdoor application, as the key feature of the AHFO is the ability to measure spatial structures in the flow, over scales ranging from one meter to several kilometers. In the future, the technique could be useful for micrometeorological and hydrological applications, allowing for characterization of spatial varying fields of mean wind speed, such as in canopy flows or in sloping terrain.

Author contributions. Justus van Ramshorst prepared and performed the experiments, worked on analyzing the data and writing the manuscript. John Selker and Chad Higgins assisted with the experiments and analyzing the data and contributed to the manuscript. Miriam Coenders-Gerrits, Bart Schilperoort, Bas van de Wiel and Jonathan Izett helped with analyzing the data and contributed to the manuscript. Huub Savenije and Nick van de Giesen contributed to the manuscript.

Competing interests. The authors declare that they have no conflict of interest.

Acknowledgements. Many thanks for the practical assistance of Cara Walter and Jim Wagner with the AHFO/DTS setup and appreciation for the people of the OPEnS LAB for assisting with the assembling of parts. This project was partly funded by NWO Earth and Life Sciences, Veni project 863.15.022, The Netherlands. We are also grateful for the funding by Holland Scholarship and CTEMPs.

Appendix A: FO cable schematization

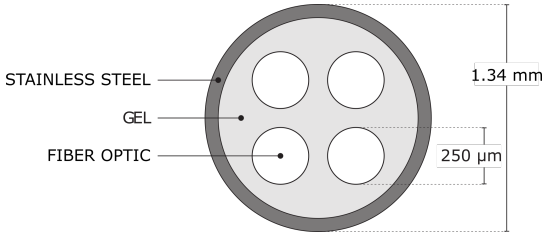

Figure A1. Cross-section of the FO cable

Appendix B: Comparison of AHFO and sonic anemometer wind speed

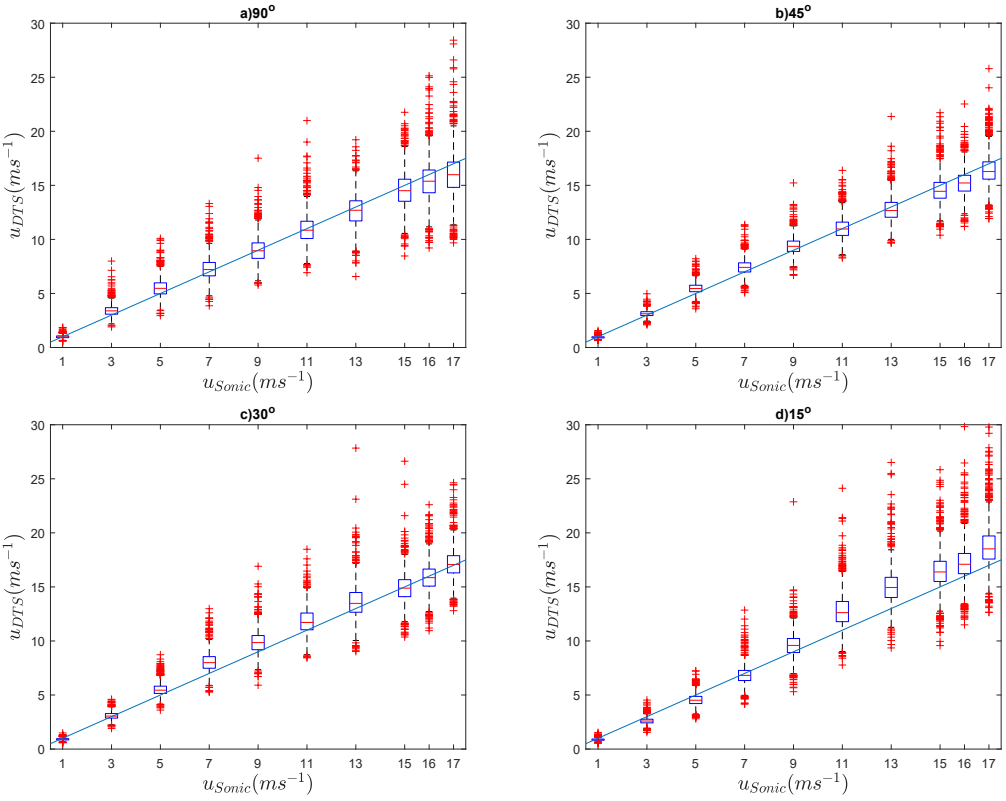

Figure B1. Comparison of AHFO and sonic anemometer wind speed at a 1-s temporal resolution, for the four different angles of attack. a) 90°(slope=0.92, intercept=0.6), b) 45°(slope=0.94, intercept=0.48), c) 30°(slope=0.99, intercept=0.42), and d) 15°(slope=1.15, intercept=-0.71). $n_{space} = 10, n_{time} = 1$. The line represents the 1:1-line.

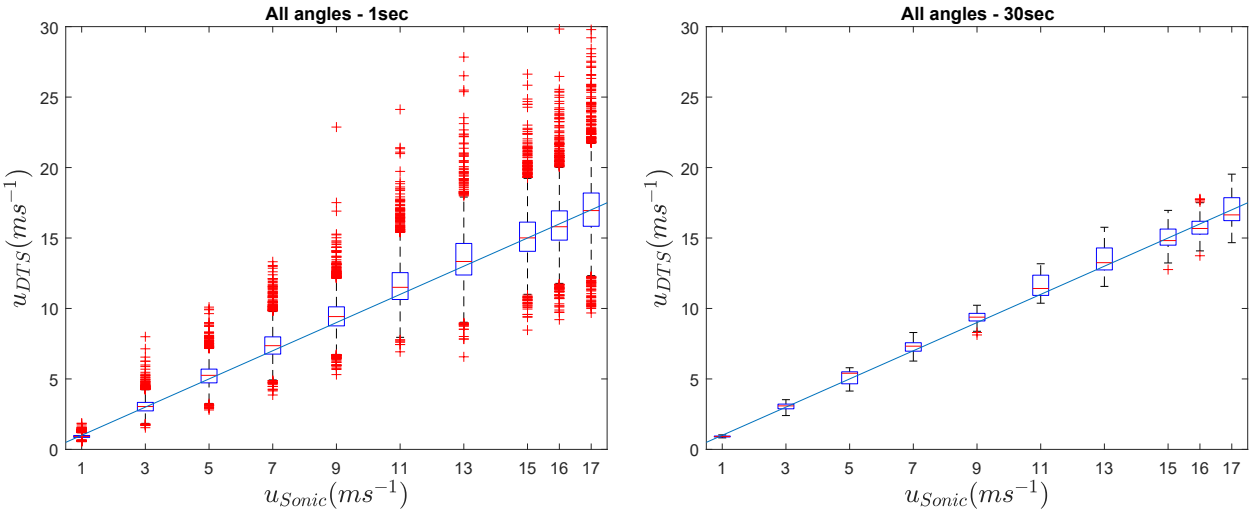

Figure B2. Comparison of AHFO and sonic anemometer wind speed~~averaged over 30 s. The boxplot includes the measurements of~~ combining all angles of attack at a 1-s(a) and 30-s(b) resolution. ~~$n_{space} = 10, n_{time} = 30$~~ $n_{space} = 10, n_{time} = 1$ and 30. The line represents the 1:1-line.

Appendix C: Wind tunnel flow characteristics

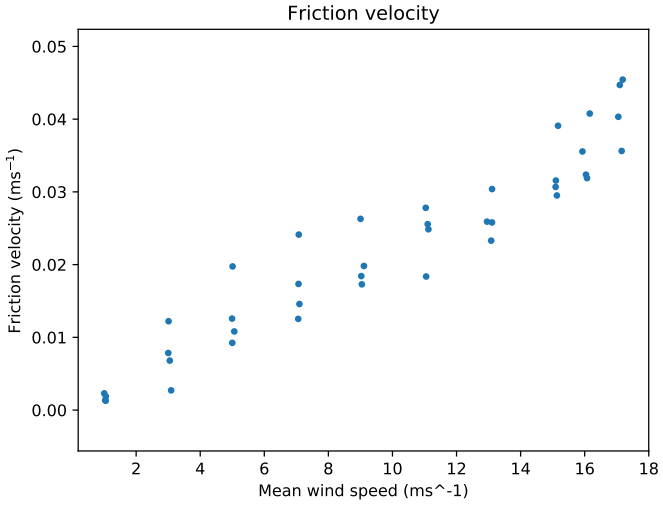

Figure C1. Friction velocity (ms^{-1}) in the wind tunnel during AHFO experiment.

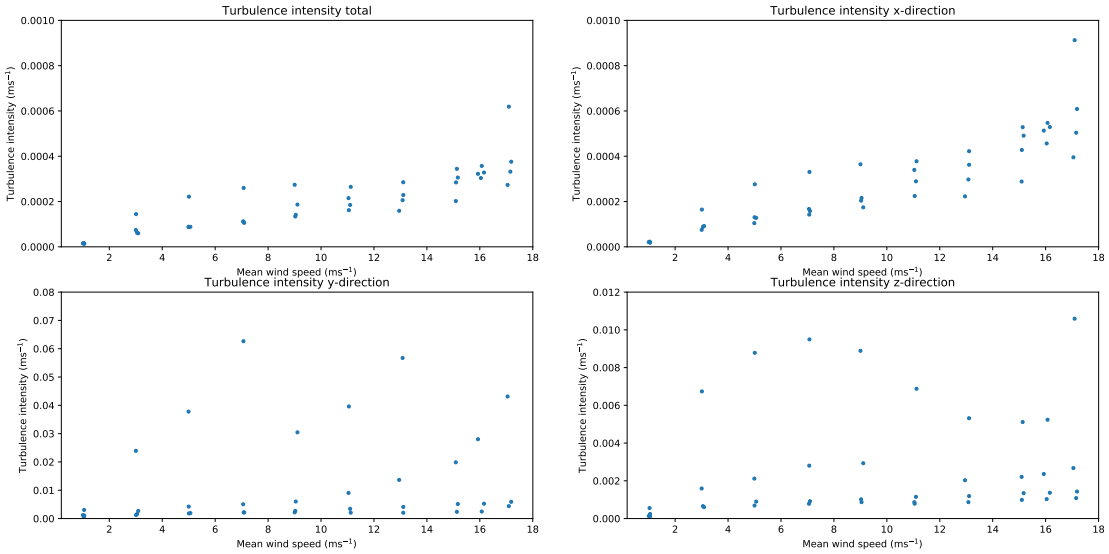

Figure C2. Turbulence intensity (variance devided by mean wind speed) (ms^{-1}) in the wind tunnel during AHFO experiment. The x-direction is in the flow direction. The y-direction is the width direction. The z-direction is the height direction.

Table D1. Standard deviation σ_{space} of 5 pairs of AHFO measurements (duplex configuration) per wind speed, and its normalized standard deviation. It shows that the normalized standard deviation is $\approx 3\%$ no matter if one takes the top, mid-top, center, mid-bottom, or bottom pair.

u (ms^{-1})	1	3	5	7	9	11	13	15	16	17
σ_{space} (ms^{-1})	0.033	0.092	0.147	0.181	0.235	0.312	0.323	0.445	0.526	0.544
Normalized σ_{space} (%)	0.033	0.031	0.029	0.026	0.026	0.028	0.025	0.030	0.033	0.032

For each angle and power rate, the u_{dts} was calculated with only the two temperature differences (duplex configuration) of the top of wind tunnel, or the mid-top, center, mid-bottom, or bottom of the wind tunnel (thus $n_{space} = 2$). From these 5 pairs we calculated the standard deviation σ_{space} per wind speed.

Appendix D: Extended spatial range

References

Adrian, R. J., Johnson, R. E., Jones, B. G., Merati, P., and Tung, A. T.: Aerodynamic disturbances of hot-wire probes and directional sensitivity, Journal of Physics E: Scientific Instruments, 17, 62–71, https://doi.org/10.1088/0022-3735/17/1/012, 1984.

Baldwin, A. J. and Lovell-Smith, J. E. R.: The emissivity of stainless steel in dairy plant thermal design, Journal of Food Engineering, 17, 281–289, https://doi.org/10.1016/0260-8774(92)90045-8, 1992.

Bentamy, A., Katsaros, K. B., Mestas-Nuñez, A. M., Drennan, W. M., Forde, E. B., and Roquet, H.: Satellite Estimates of Wind Speed and Latent Heat Flux over the Global Oceans, Journal of Climate, 16, 637–656, https://doi.org/10.1175/1520-0442(2003)016<0637:SEOWSA>2.0.CO;2, 2003.

Bou-Zeid, E., HIGGINS, C., HUWALD, H., MENEVEAU, C., and PARLANGE, M. B.: Field study of the dynamics and modelling of subgrid-scale turbulence in a stable atmospheric surface layer over a glacier, Journal of Fluid Mechanics, 665, 480–515, https://doi.org/10.1017/S0022112010004015, http://www.journals.cambridge.org/abstract{_}S0022112010004015, 2010.

Bruun, H. H.: Interpretation of a Hot Wire Signal Using a Universal Calibration Law., Journal of Physics E: Scientific Instruments, 4, 225–231, https://doi.org/10.1088/0022-3735/4/3/016, 1971.

Cengel, Y. and Ghajar, A.: Heat and mass transfer: fundamentals and applications, McGraw-Hill Higher Education, 2014.

Euser, T., Luxemburg, W. M. J., Everson, C. S., Mengistu, M. G., Clulow, A. D., and Bastiaanssen, W. G. M.: A new method to measure Bowen ratios using high-resolution vertical dry and wet bulb temperature profiles, Hydrology and Earth System Sciences, 18, 2021–2032, https://doi.org/10.5194/hess-18-2021-2014, 2014.

Goodberlet, M. A., Swift, C. T., and Wilkerson, J. C.: Remote sensing of ocean surface winds with the special sensor microwave/imager, Journal of Geophysical Research, 94, 14 547–14 555, https://doi.org/10.1029/JC094iC10p14547, 1989.

Ha, K.-J., Hyun, Y.-K., Oh, H.-M., Kim, K.-E., and Mahrt, L.: Evaluation of Boundary Layer Similarity Theory for Stable Conditions in CASES-99, Monthly Weather Review, 135, 3474–3483, https://doi.org/10.1175/MWR3488.1, http://journals.ametsoc.org/doi/abs/10.1175/MWR3488.1, 2007.

Hausner, M. B., Suárez, F., Glander, K. E., van de Giesen, N., Selker, J. S., and Tyler, S. W.: Calibrating single-ended fiber-optic raman spectra distributed temperature sensing data, Sensors, 11, 10 859–10 879, https://doi.org/10.3390/s111110859, 2011.

Higgins, C. W., Meneveau, C., and Parlange, M. B.: Geometric Alignments of the Subgrid-Scale Force in the Atmospheric Boundary Layer, Boundary-Layer Meteorology, 132, 1–9, https://doi.org/10.1007/s10546-009-9385-3, https://doi.org/10.1007/s10546-009-9385-3, 2009.

Higgins, C. W., Froidevaux, M., Simeonov, V., Vercauteren, N., Barry, C., and Parlange, M. B.: The Effect of Scale on the Applicability of Taylor's Frozen Turbulence Hypothesis in the Atmospheric Boundary Layer, Boundary-Layer Meteorology, 143, 379–391, https://doi.org/10.1007/s10546-012-9701-1, 2012.

Higgins, C. W., Wing, M. G., Kelley, J., Sayde, C., Burnett, J., and Holmes, H. A.: A high resolution measurement of the morning ABL transition using distributed temperature sensing and an unmanned aircraft system, Environmental Fluid Mechanics, 18, 683–693, https://doi.org/10.1007/s10652-017-9569-1, https://doi.org/10.1007/s10652-017-9569-1, 2018.

Hinze, J.: Turbulence, McGraw-Hill Higher Education, New York, 1975.

Holtslag, A. A., Svensson, G., Baas, P., Basu, S., Beare, B., Beljaars, A. C., Bosveld, F. C., Cuxart, J., Lindvall, J., Steeneveld, G. J., Tjernström, M., and Van De Wiel, B. J.: Stable atmospheric boundary layers and diurnal cycles: Challenges for weather and climate models, Bulletin of the American Meteorological Society, 94, 1691–1706, https://doi.org/10.1175/BAMS-D-11-00187.1, 2013.

Izett, J. G., Schilperoort, B., Coenders-Gerrits, M., Baas, P., Bosveld, F. C., and van de Wiel, B. J. H.: Missed Fog?, Boundary-Layer Meteorology, https://doi.org/10.1007/s10546-019-00462-3, http://link.springer.com/10.1007/s10546-019-00462-3, 2019.

Jong, S. A. P. D., Slingerland, J. D., and Giesen, N. C. V. D.: Fiber optic distributed temperature sensing for the determination of air temperature, pp. 335–339, https://doi.org/10.5194/amt-8-335-2015, 2015.

Kaiser, R. and Knight, W.: Digital signal averaging, Journal of Magnetic Resonance (1969), 36, 215–220, https://doi.org/10.1016/0022-2364(79)90096-9, http://linkinghub.elsevier.com/retrieve/pii/0022236479900969, 1979.

Keller, C. A., Huwald, H., Vollmer, M. K., Wenger, A., Hill, M., Parlange, M. B., and Reimann, S.: Fiber optic distributed temperature sensing for the determination of the nocturnal atmospheric boundary layer height, Atmospheric Measurement Techniques, 4, 143–149, https://doi.org/10.5194/amt-4-143-2011, http://www.atmos-meas-tech.net/4/143/2011/, 2011.

Kelly, M., Wyngaard, J. C., and Sullivan, P. P.: Application of a Subfilter-Scale Flux Model over the Ocean Using OHATS Field Data, Journal of the Atmospheric Sciences, 66, 3217–3225, https://doi.org/10.1175/2009JAS2903.1, http://journals.ametsoc.org/doi/abs/10.1175/2009JAS2903.1, 2009.

Madhusudana, C.: Accuracy in thermal contact conductance experiments - the effect of heat losses to the surroundings, International Communications in Heat and Mass Transfer, 27, 877–891, https://doi.org/10.1016/S0735-1933(00)00168-8, http://linkinghub.elsevier.com/retrieve/pii/S0735193300001688, 2000.

Patton, E. G., Horst, T. W., Sullivan, P. P., Lenschow, D. H., Oncley, S. P., Brown, W. O. J., Burns, S. P., Guenther, A. B., Held, A., Karl, T., Mayor, S. D., Rizzo, L. V., Spuler, S. M., Sun, J., Turnipseed, A. A., Allwine, E. J., Edburg, S. L., Lamb, B. K., Avissar, R., Calhoun, R. J., Kleissl, J., Massman, W. J., Paw U, K. T., and Weil, J. C.: The Canopy Horizontal Array Turbulence Study, Bulletin of the American Meteorological Society, 92, 593–611, https://doi.org/10.1175/2010BAMS2614.1, http://journals.ametsoc.org/doi/abs/10.1175/2010BAMS2614.1, 2011.

Perry, A.: Hot-wire anemometry, Clarendon press, Oxford, UK, 1982.

Petrides, A. C., Huff, J., Arik, A., van de Giesen, N., Kennedy, A. M., Thomas, C. K., and Selker, J. S.: Shade estimation over streams using distributed temperature sensing, Water Resources Research, 47, https://doi.org/10.1029/2010WR009482, http://doi.wiley.com/10.1029/2010WR009482, 2011.

Sayde, C., Buelga, J. B., Rodriguez-Sinobas, L., El Khoury, L., English, M., van de Giesen, N., and Selker, J. S.: Mapping variability of soil water content and flux across 1-1000 m scales using the Actively Heated Fiber Optic method, Water Resources Research, 50, 7302–7317, https://doi.org/10.1002/2013WR014983, http://doi.wiley.com/10.1002/2013WR014983, 2014.

Sayde, C., Thomas, C. K., Wagner, J., and Selker, J.: High-resolution wind speed measurements using actively heated fiber optics, Geophysical Research Letters, 42, 10 064–10 073, https://doi.org/10.1002/2015GL066729, 2015.

Schilperoort, B., Coenders-Gerrits, M., Luxemburg, W., Jiménez Rodríguez, C., Cisneros Vaca, C., and Savenije, H.: Technical note: Using distributed temperature sensing for Bowen ratio evaporation measurements, Hydrology and Earth System Sciences, 22, 819–830, https://doi.org/10.5194/hess-22-819-2018, https://www.hydrol-earth-syst-sci.net/22/819/2018/, 2018.

Selker, J., van de Giesen, N. C., Westhoff, M., Luxemburg, W., and Parlange, M. B.: Fiber optics opens window on stream dynamics, Geophysical Research Letters, 33, 27–30, https://doi.org/10.1029/2006GL027979, 2006a.

Selker, J. S., Thévenaz, L., Huwald, H., Mallet, A., Luxemburg, W., Van De Giesen, N., Stejskal, M., Zeman, J., Westhoff, M., and Parlange, M. B.: Distributed fiber-optic temperature sensing for hydrologic systems, Water Resources Research, 42, 1–8, https://doi.org/10.1029/2006WR005326, 2006b.

Steele-Dunne, S. C., Rutten, M. M., Krzeminska, D. M., Hausner, M., Tyler, S. W., Selker, J., Bogaard, T. A., and van de Giesen, N. C.: Feasibility of soil moisture estimation using passive distributed temperature sensing, Water Resources Research, 46, https://doi.org/10.1029/2009WR008272, http://doi.wiley.com/10.1029/2009WR008272, 2010.

Taylor, G. I.: The Spectrum of Turbulence, Proceedings of the Royal Society A: Mathematical, Physical and Engineering Sciences, 164, 476–490, https://doi.org/10.1098/rspa.1938.0032, http://rspa.royalsocietypublishing.org/cgi/doi/10.1098/rspa.1938.0032, 1938.

Thomas, C. K., Kennedy, A. M., Selker, J. S., Moretti, A., Schroth, M. H., Smoot, A. R., Tufillaro, N. B., and Zeeman, M. J.: High-Resolution Fibre-Optic Temperature Sensing: A New Tool to Study the Two-Dimensional Structure of Atmospheric Surface-Layer Flow, Boundary-Layer Meteorology, 142, 177–192, https://doi.org/10.1007/s10546-011-9672-7, 2012.

Tsilingiris, P.: Thermophysical and transport properties of humid air at temperature range between 0 and 100°C, Energy Conversion and Management, 49, 1098–1110, https://doi.org/10.1016/j.enconman.2007.09.015, http://linkinghub.elsevier.com/retrieve/pii/S0196890407003329, 2008.

Tyler, S. W., Burak, S. A., McNamara, J. P., Lamontagne, A., Selker, J. S., and Dozier, J.: Spatially distributed temperatures at the base of two mountain snowpacks measured with fiber-optic sensors, Journal of Glaciology, 54, 673–679, https://doi.org/10.3189/002214308786570827, https://www.cambridge.org/core/product/identifier/S0022143000208770/type/journal{_}article, 2008.

Tyler, S. W., Selker, J. S., Hausner, M. B., Hatch, C. E., Torgersen, T., Thodal, C. E., and Schladow, S. G.: Environmental temperature sensing using Raman spectra DTS fiber-optic methods, Water Resources Research, 45, 1–11, https://doi.org/10.1029/2008WR007052, http://doi.wiley.com/10.1029/2008WR007052, 2009.

van de Giesen, N., Steele-Dunne, S. C., Jansen, J., Hoes, O., Hausner, M. B., Tyler, S., and Selker, J.: Double-ended calibration of fiber-optic raman spectra distributed temperature sensing data, Sensors (Switzerland), 12, 5471–5485, https://doi.org/10.3390/s120505471, 2012.

Webster, C. A. G.: A note on the sensitivity to yaw of a hot-wire anemometer, Journal of Fluid Mechanics, 13, 307, https://doi.org/10.1017/S0022112062000695, http://www.journals.cambridge.org/abstract{_}S0022112062000695, 1962.

Zeeman, M. J., Selker, J. S., and Thomas, C. K.: Near-Surface Motion in the Nocturnal, Stable Boundary Layer Observed with Fibre-Optic Distributed Temperature Sensing, Boundary-Layer Meteorology, 154, 189–205, https://doi.org/https://doi.org/10.1007/s10546-014-9972-9, 2015.

Žukauskas, A.: Heat Transfer from Tubes in Crossflow, pp. 93–160, https://doi.org/10.1016/S0065-2717(08)70038-8, http://linkinghub.elsevier.com/retrieve/pii/S0065271708700388, 1972.